Journal of The Electrochemical Society, **156** (7) B862-B869 (2009)
0013-4651/2009/156(7)/B862/8/$25.00 © The Electrochemical Society

Effect of SnO_2 Deposition Sequence in SnO_2-Modified PtRu/C Catalyst Preparation on Catalytic Activity for Methanol Electro-Oxidation

Guoxiong Wang,[a,z] Tatsuya Takeguchi,[a,*,z] Yi Zhang,[a] Ernee Noryana Muhamad,[a] Masahiro Sadakane,[a] Shen Ye,[a,b] and Wataru Ueda[a]

[a]*Catalysis Research Center, Hokkaido University, Sapporo 001-0021, Japan*
[b]*PRESTO, Japan Science and Technology Agency (JST), Tokyo 102-0075, Japan*

SnO_2-modified PtRu/C catalysts were prepared in a polyol process to investigate the effect of a SnO_2 deposition sequence on the catalytic activity for methanol electro-oxidation. The structure, morphology, and chemical state of the prepared catalysts were characterized by X-ray diffraction, scanning transmission electron microscopy, and X-ray photoelectron spectroscopy. The electrochemical activities were evaluated by cyclic voltammetry, linear sweep voltammetry, and chronoamperometry measurements in combination with in situ IR reflection–absorption spectroscopy (IRRAS). Compared with those in the PtRu/C catalyst, a simultaneous deposition of PtRu and SnO_2 particles or a deposition of SnO_2 prior to PtRu improved the metal dispersion and decreased the alloyed Ru fraction. The deposition sequence of SnO_2 did not alter the chemical-state distribution of Pt and Ru but resulted in a different surface atomic ratio of Pt, Ru, and SnO_2. Electrochemical and in situ IRRAS measurements indicated that the SnO_2-modified PtRu/C catalyst prepared by the deposition of PtRu prior to SnO_2 gave the best catalytic activity for CO_{ads} and methanol electro-oxidation among the PtRu/C and SnO_2-modified PtRu/C catalysts. The roles of SnO_2 deposited with different sequences in the SnO_2-modified PtRu/C catalysts were proposed.
 [DOI: 10.1149/1.3133249]

Manuscript submitted February 2, 2009; revised manuscript received April 10, 2009. Published May 21, 2009.

The electro-oxidation of methanol has attracted considerable interest due to its importance for direct methanol fuel cells (DMFCs), and the PtRu/C catalyst has been recognized as the most active binary catalyst.[1] The enhanced performance on the PtRu/C catalyst is usually explained by a bifunctional mechanism,[2-4] where methanol is adsorbed and dehydrogenated to produce CO_{ads} on Pt active sites, Ru is more active than Pt to provide OH_{ads} at low potentials by a water-discharge reaction, and CO_{ads} on Pt active sites reacts with the neighboring OH_{ads} to yield CO_2. A PtRu alloy is also thought to weaken CO adsorption on Pt active sites by the electronic effect.[5-7] However, the slow kinetics of methanol electro-oxidation at low temperatures is still an obstacle for further development of DMFCs.

To improve the catalytic activity for methanol electro-oxidation, several PtRu-based ternary catalysts, such as PtRuIr, PtRuSn, PtRuFe, and PtRuPd, were investigated.[8-14] The third metal was added into PtRu by co-reduction of their corresponding precursors, and the third metal was presented as a mixture of alloy and metal oxide forms in the PtRu-based ternary catalyst. Although the catalytic activity for methanol electro-oxidation was improved, it had been difficult to distinguish the individual roles of alloyed and oxide forms of the third metal. Another slightly different approach is adding a metal oxide into PtRu to form a ternary $PtRuMeO_x$ catalyst.[15,16] Martínez-Huerta et al. prepared a $PtRu/MoO_x/C$ catalyst by a two-step procedure: Molybdenum oxide was first deposited on a carbon substrate to form MoO_x/C by an impregnation method, and then Pt and Ru were deposited onto MoO_x/C by a colloid method. Cyclic voltammetry (CV) and chronoamperometry measurements indicated that the catalytic activity for methanol electro-oxidation on the $PtRu/MoO_x/C$ catalyst was greatly improved.[16]

It has been reported that SnO_2 adjacent to Pt can promote CO_{ads} electro-oxidation by providing OH_{ads} at low potentials via the bifunctional mechanism.[17,18] According to CO stripping voltammetry results, the $PtSnO_2/C$ catalyst presented a much negative shift in the onset potential compared with the PtRu/C catalyst; however, the oxidation current on the PtRu/C catalyst increased more rapidly with potential than that on the $PtSnO_2/C$ catalyst, suggesting that Ru is more effective than SnO_2 in promoting CO_{ads} electro-oxidation at relatively high potentials.[18,19] For the ternary PtRuSn/C catalyst previously reported, Sn is mainly present in the oxidized state on the catalyst surface, and the improvement in the catalytic activity for methanol electro-oxidation is usually ascribed to the synergistic effect of SnO_2 and Ru species.[10] However, the catalytic activity of the PtRuSn/C catalyst is also reported to be inferior to that of the PtRu/C catalyst because SnO_2 that covers with Pt sites blocks the adsorption of methanol and is detrimental to the catalytic activity.[10,20] Therefore, to minimize the blockage effect of SnO_2 and to optimize the catalytic activity, the addition mode of SnO_2 to PtRu needs to be urgently investigated.

In this work, SnO_2-modified PtRu/C catalysts with three kinds of SnO_2 deposition sequences were prepared in a polyol process, and the effect of the SnO_2 deposition sequence was investigated by evaluating the catalytic activity for methanol electro-oxidation. The prepared catalysts were characterized by X-ray diffraction (XRD), scanning transmission electron microscopy (STEM), and X-ray photoelectron spectroscopy (XPS). CO stripping voltammetry was conducted to evaluate the CO_{ads} electro-oxidation activity on the catalysts as well as the electrochemical surface area of the catalysts. Conventional electrochemical techniques, in combination with in situ IR reflection–absorption spectroscopy (IRRAS), were applied to compare the electrochemical performance of the SnO_2-modified PtRu/C catalysts for methanol electro-oxidation.

Experimental

Catalyst preparation.— PtRu and SnO_2 colloids were prepared separately in a polyol process under air atmosphere as described below.[21,22] (*i*) PtRu colloid: Calculated amounts of $H_2PtCl_6 \cdot 6H_2O$ (Wako Pure Chemical Industries, Ltd.) and $RuCl_3 \cdot xH_2O$ (Nakarai Chemicals, Ltd.) were dissolved in ethylene glycol (Wako Pure Chemical Industries, Ltd.) in a three-necked flask to form a brown solution with a 2 mg (Pt + Ru) mL^{-1} solvent. Then the pH value of the solution was increased to about 13 with a 1 M NaOH (Wako Pure Chemical Industries, Ltd.) solution. The solution was heated to 170°C at a rate of 10°C min^{-1} and kept at that temperature for 4 h, and then the PtRu colloid solution was cooled to 90°C. (*ii*) SnO_2 colloid: A calculated amount of $SnCl_2 \cdot 2H_2O$ was added to ethylene glycol to form a clear solution with a concentration of about 0.5 mg Sn^{2+} mL^{-1} solvent, and the solution was heated to 190°C at a rate of 10°C min^{-1}, kept at that temperature for 0.5 h, and then cooled to 90°C.

Three SnO_2-modified PtRu/C catalysts were prepared by varying the deposition sequences of SnO_2: (*i*) PtRu and SnO_2 colloids were mixed for 2 h and then codeposited onto Vulcan XC-72 carbon

* Electrochemical Society Active Member.
z E-mail: wanggx@cat.hokudai.ac.jp; takeguch@cat.hokudai.ac.jp

support (Cabot Corp.) by adjusting the pH value of the synthesis solution to about 2. After the solution had been stirred for 24 h at 90°C, the obtained catalyst was filtered and washed thoroughly with distilled water, followed by drying in N_2 at 80°C for 10 h. The prepared catalyst was denoted as the $PtRuSnO_2/C$ catalyst. (*ii*) The SnO_2 colloid was first deposited onto Vulcan XC-72 carbon support to obtain SnO_2/C by adjusting the pH value of the synthesis solution to about 2, followed by washing and drying, and then the PtRu colloid was deposited onto SnO_2/C in the same manner. The prepared catalyst was denoted as the $PtRu/SnO_2/C$ catalyst. (*iii*) The PtRu and SnO_2 colloids were deposited onto carbon support in the reverse order with the $PtRu/SnO_2/C$ catalyst, and the prepared catalyst was denoted as the $SnO_2/PtRu/C$ catalyst. In all of the SnO_2-modified PtRu/C catalysts, PtRu loading was 45 wt % and the atomic ratio of Pt:Ru:SnO_2 was 3:3:1. For comparison, 45 wt % PtRu/C (Pt:Ru = 1:1) was also prepared in the polyol process.

Physicochemical characterization.— The XRD patterns of PtRu/C and SnO_2-modified PtRu/C catalysts were recorded with a powder X-ray diffractometer (Rigaku, RINT 2000) using Cu Kα radiation with a Ni filter. The tube current was 40 mA with a tube voltage of 40 kV. The angle was extended from 10 to 85° at a step size of 0.01°, accumulating data for 6 s per step. The peak profile of the (220) reflection of the Pt face-centered cubic structure was fitted to a Gaussian line shape so that the position of the peak maximum ($2\theta_{max}$) could be obtained precisely for the alloying degree calculation. Catalyst morphology was investigated by using an STEM (Hitachi HD-2000) at 200 kV and 30 μA, and more than 200 particles were calculated to obtain the average particle size and particle-size distribution of the catalysts. XPS measurements were carried out using a JEOL JPS-9010MC spectrometer with a Mg Kα radiation source. The Pt 4f and Ru 3p signals were collected and analyzed by the deconvolution of the spectra using the free software XPSPeak. The position of the C 1s peak, that is, 284.2 eV for the JEOL JPS-9010MC spectrometer, was used to correct the binding energies of the catalysts.

Electrochemical measurements.— Electrochemical measurements were carried out in a 250 mL three-electrode cell (HR200, Hokuto Denko Corp.) at 25°C. A commercial glassy carbon (GC) electrode (HR2-D1-GC-5, 5 mm in diameter, 0.196 cm^2, Hokuto Denko Corp.), a Pt-wire electrode (Hokuto Denko Corp.), and a saturated calomel electrode (Hokuto Denko Corp.) were used as a working electrode, a counter electrode, and a reference electrode, respectively. The potential of the working electrode was controlled by an Iviumstat Electrochemical Interface System (Ivium Technologies B.V.). Five milligrams of the catalyst was dispersed in a mixture of 2 mL water, 2 mL ethanol, and 50 μL Nafion solution (5 wt %, Aldrich) with ultrasonic stirring to form a homogeneous ink.[19] The catalyst layer was prepared by dropping 20 μL of the ink onto a GC disk electrode by a microsyringe and drying at room temperature. All potential values in this paper are referred to a reversible hydrogen electrode. For CO stripping voltammetry, pure CO was supplied into the electrolyte solution (0.5 M $HClO_4$) for 20 min at a fixed potential of 0.018 V,[23] and then high purity (99.99%) Ar was bubbled for 30 min to remove the CO dissolved in the electrolyte solution. The current-potential cycles were obtained from 0.018 to 1.2 V at a scan rate of 10 mV s^{-1}. The calculated peak charge Q_{CO} was used to compare the electrochemical surface area of the catalysts, which was obtained with the assumption of a monolayer of linearly adsorbed CO and charge density required for the electro-oxidation of 0.42 mC cm^{-2}.[24]

The CVs of methanol electro-oxidation were measured in a potential range of 0–1.0 V at 25°C in a 0.5 M $HClO_4$ + 0.5 M CH_3OH solution saturated with high purity Ar gas, and the scan rate was 20 mV s^{-1}. The linear sweep voltammetries (LSVs) of methanol electro-oxidation were recorded from 0 to 0.6 V at a scan rate of 1 mV s^{-1}. The chronoamperometry curves were obtained by polarizing the electrode at 0.55 V for 900 s in the above-mentioned electrolyte solution. For all of the electrochemical results, the current density was normalized according to the corresponding electrochemical surface area of the catalyst.

The in situ IRRAS measurements were carried out in a homemade poly(tetrafluoroethylene) cell with a CaF_2 optical window using a Bio-Rad FTS-60A/896 spectrometer equipped with a mercury cadmium telluride detector cooled by liquid nitrogen.[25-27] A gold disk (10 mm in diameter) was used as an electrode substrate for IRRAS measurements. Before the IRRAS measurement, the electrode was polished with alumina (0.5 μm) and rinsed with Milli-Q water. The catalyst layers were deposited on the gold electrode surface, which is inert to methanol electro-oxidation, with the same method as that described for the CO stripping experiments. The electrode was pushed onto the window with the thin-layer geometry to reduce the IR absorption by the aqueous solution. The in situ IR spectra were recorded with a potential scan rate of 5 mV s^{-1}, and 14 interferograms were co-added to each spectrum in 2 s. All the IR spectra were normalized to a reference spectrum recorded at 0.05 V in the 0.5 M $HClO_4$ + 0.5 M CH_3OH solution in the unit of absorbance.

Results and Discussion

XRD and STEM characterization.— The XRD patterns of PtRu/C and different SnO_2-modified PtRu/C catalysts are shown in Fig. 1. The broad peak at around 26° is associated with the (002) diffraction peak of the Vulcan XC-72 carbon support. Compared with the PtRu/C catalyst, two additional weak diffraction peaks at around 34 and 52° can be observed in the SnO_2-modified PtRu/C catalysts, these peaks being related to SnO_2(101) and SnO_2(211) planes, respectively. PtRu/C and SnO_2-modified PtRu/C catalysts display a positive shift in Pt diffraction peaks, which possibly originates from the PtRu alloy formation.[28] As shown in Fig. 1b, the Pt(220) peak position ($2\theta_{max}$) was obtained from curve fitting and used for the calculation of the lattice parameter (a)

$$a = \frac{\sqrt{2}\lambda_{K\alpha}}{\sin\ \theta_{max}} \quad [1]$$

The alloying degree of the PtRu/C catalyst is defined as the Ru atomic fraction (χ_{Ru}) in the PtRu alloy,[28] which is related to the lattice parameter by the following equation proposed by Antolini and Cardellini[29]

$$a = a_o - 0.124\chi_{Ru} \quad [2]$$

where a_o = 0.39155 nm is the lattice parameter of carbon-supported platinum. For the PtRu/C alloy catalyst with an atomic ratio of 1:1, the theoretical value of χ_{Ru} is 0.5. The alloying degree of the PtRu/C catalyst was calculated to be 0.17, which is similar to the reported result.[30] Although the PtRu colloid was prepared by co-reduction of Pt and Ru precursors in the polyol process, the majority of the PtRu nanoparticles still existed as separate Pt and Ru phases in the colloid solution.[30] After decreasing the pH value to about 2, the stability of the PtRu colloid was destroyed;[21,30] consequently, the Pt and Ru particles were deposited onto the carbon support. The Pt and Ru particles on the carbon support are thought to be in close contact with each other due to the homogeneous mixing in the PtRu colloid solution. The alloying degree of the SnO_2-modified PtRu/C catalysts changes with the SnO_2 deposition sequence. The $PtRuSnO_2/C$ catalyst has the lowest alloying degree of 0.05, and this result suggested that PtRu alloy formation was affected by the codeposition of PtRu and SnO_2 particles. When the PtRu and SnO_2 colloids were mixed homogeneously and then codeposited onto the carbon support, the addition of SnO_2 lowered the contact between Pt and Ru particles and resulted in a poor PtRu alloy formation. The alloying degree of the $PtRu/SnO_2/C$ catalyst is also poorer than that of the PtRu/C catalyst, suggesting that prior deposition of the SnO_2 particles onto the carbon support still had a negative effect on the PtRu alloy formation. For the $SnO_2/PtRu/C$ catalyst, SnO_2 deposition did not affect the intimate contact of Pt and Ru particles, and the alloying

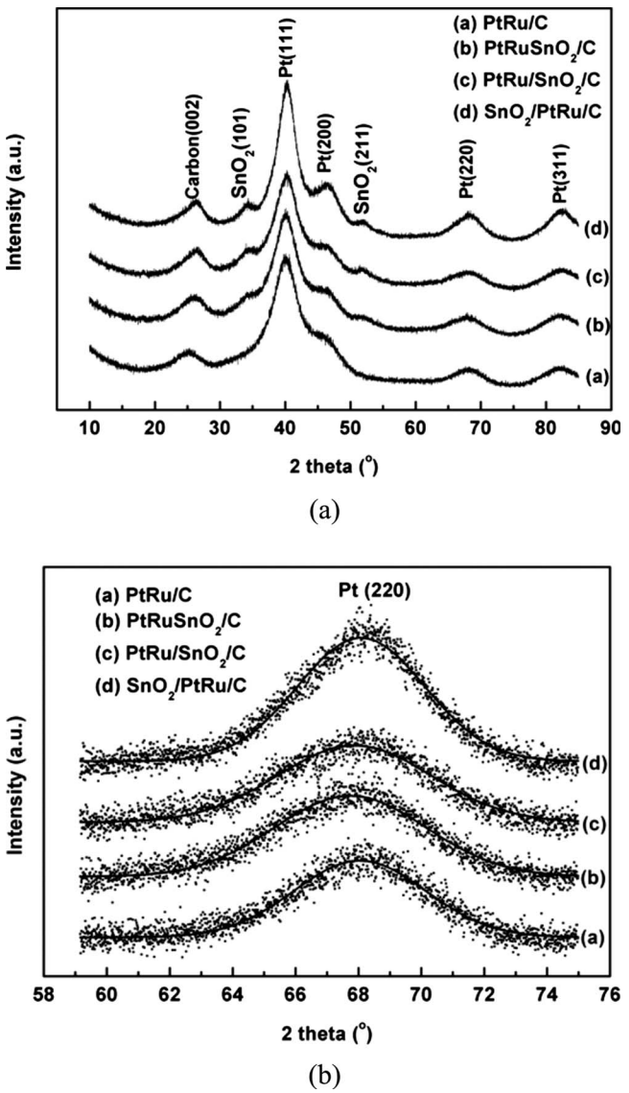

Figure 1. XRD patterns of PtRu/C and different SnO_2-modified PtRu/C catalysts.

degree of the SnO_2/PtRu/C catalyst is slightly greater than that of the PtRu/C catalyst, which is probably due to a greater PtRu deposition density on the carbon support prior to SnO_2 deposition.

The mean crystallite size of the catalysts was also calculated from the Pt(220) diffraction peak via the Scherrer equation, and the results are listed in Table I. The mean crystallite size decreased from 1.9 to 1.7 nm in the simultaneous deposition of SnO_2 and PtRu particles or in the deposition of SnO_2 prior to PtRu, which might be explained by the fact that SnO_2 in the colloid solution or deposited on the carbon support could act as a separator, inhibiting the agglomeration of PtRu particles during the deposition process. The mean crystallite size of the SnO_2/PtRu/C catalyst increased slightly to 2.0 nm due to a greater PtRu loading on the carbon support prior to SnO_2 deposition.

Figure 2 shows STEM images and the corresponding histograms of the particle-size distribution of PtRu/C and different SnO_2-modified PtRu/C catalysts. All of the catalysts have similar morphologies with a uniform distribution on the carbon support. Among the four catalysts, the PtRu/SnO_2/C catalyst has an average particle size of 2.2 nm with the narrowest size distribution, while the SnO_2/PtRu/C catalyst has a relatively large particle size of 2.7 nm with the broadest size distribution, which agree with the XRD results. It should be noted that it is difficult to distinguish SnO_2 particles in the STEM images due to the similar size of PtRu and SnO_2 particles obtained in the polyol process.[21,22] The small particle size of PtRu/C and SnO_2-modified PtRu/C catalysts ranging from 2.2 to 2.7 nm is an important factor for obtaining a high level of catalytic activity for CO_{ads} and methanol electro-oxidation.

CO stripping voltammetry measurement.— Figure 3 shows the CO stripping voltammetries of PtRu/C and different SnO_2-modified PtRu/C catalysts. For the PtRu/C catalyst, CO_{ads} is electro-oxidized in a relatively sharp stripping peak centered at 0.502 V. On the PtRuSnO_2/C and PtRu/SnO_2/C catalysts, CO_{ads} is electro-oxidized over a broad potential region with a peak at 0.497 and 0.494 V, respectively, while the SnO_2/PtRu/C catalyst exhibits a similarly sharp stripping peak with a negative shift of 0.024 V in peak potential. This result indicated that the CO_{ads} electro-oxidation activity was improved by the interaction between PtRu and SnO_2 particles via the bifunctional mechanism. It is obvious that the SnO_2/PtRu/C catalyst showed the most pronounced promotional effect on CO_{ads} electro-oxidation among the three SnO_2-modified PtRu/C catalysts.

The PtRu utilization is defined as the ratio between the electrochemical surface area (S_E) determined by CO stripping voltammetry and the geometrical surface area (S_G) determined by the average particle size from the STEM image, as listed in Table I. The PtRu utilization can be regarded as a measure of the fraction of the PtRu surface covered by SnO_2.[18] The PtRuSnO_2/C catalyst has the lowest PtRu metal utilization and alloying degree, indicating that the addition of SnO_2 in the PtRuSnO_2/C catalyst lowered the contact between Pt and Ru particles in the manner of SnO_2 particles covering Pt or Ru particles. The PtRu utilization in the SnO_2/PtRu/C catalyst was much greater than that in the PtRuSnO_2/C catalyst and slightly lower than that in the PtRu/C catalyst. Considering that the SnO_2/PtRu/C catalyst showed the most negative shift in peak potential for CO_{ads} electro-oxidation, SnO_2 particles in the SnO_2/PtRu/C catalyst were thought to be in contact with PtRu particles, rather than cover a large fraction of PtRu particles.

Table I. Physical characteristics and surface areas of PtRu/C and different SnO_2-modified PtRu catalysts.

Catalyst	Lattice parameter (Å)	χ_{Ru}	Mean particle size XRD (nm)	Mean particle size STEM (nm)	S_G [a] ($m^2\ g^{-1}$)	S_E [b] ($m^2\ g^{-1}$)	PtRu utilization (%)
PtRu/C	3.8939	0.17	1.9	2.5	112.1	68.1	60.7
PtRuSnO_2/C	3.9093	0.05	1.7	2.2	127.4	59.8	46.9
PtRu/SnO_2/C	3.9029	0.10	1.7	2.2	127.4	69.1	54.2
SnO_2/PtRu/C	3.8919	0.19	2.0	2.7	103.8	59.3	57.1

[a] On the basis of the average particle size from the STEM image.
[b] Calculated from the CO_{ads} stripping charge.

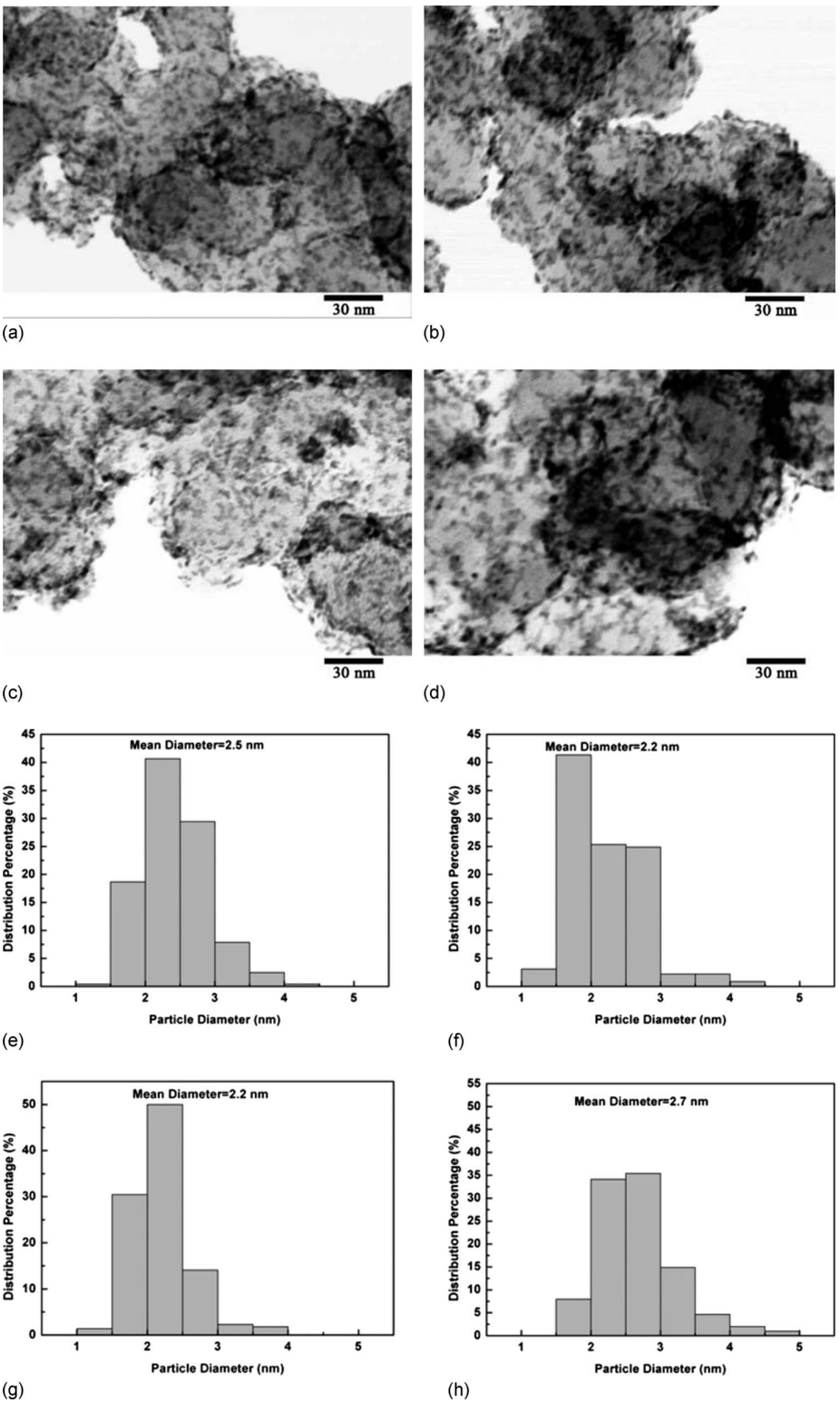

Figure 2. STEM images and the corresponding histograms of particle-size distribution of [(a) and (e)] PtRu/C, [(b) and (f)] $PtRuSnO_2/C$, [(c) and (g)] $PtRu/SnO_2/C$, and [(d) and (h)] $SnO_2/PtRu/C$ catalysts.

Electrochemical measurement of methanol electro-oxidation.— The catalytic activities for methanol electro-oxidation of the catalysts were characterized by CV, LSV, and chronoamperometry in a solution of 0.5 M $HClO_4$ + 0.5 M CH_3OH at 25°C. Figure 4 shows the sixth circle of CVs. Compared with the PtRu/C catalyst, the $PtRuSnO_2/C$ catalyst showed a positive shift of 0.041 V in peak potential, which also suggested that Pt and Ru particles covered by SnO_2 particles in the $PtRuSnO_2/C$ catalyst were not beneficial for methanol adsorption and electro-oxidation. The $PtRu/SnO_2/C$ and $SnO_2/PtRu/C$ catalysts showed a similar peak potential with the PtRu/C catalyst, and the current density of methanol electro-oxidation on the $PtRu/SnO_2/C$ and $SnO_2/PtRu/C$ catalysts was obviously greater than that on the PtRu/C catalyst.

To validate the onset potential of methanol electro-oxidation on

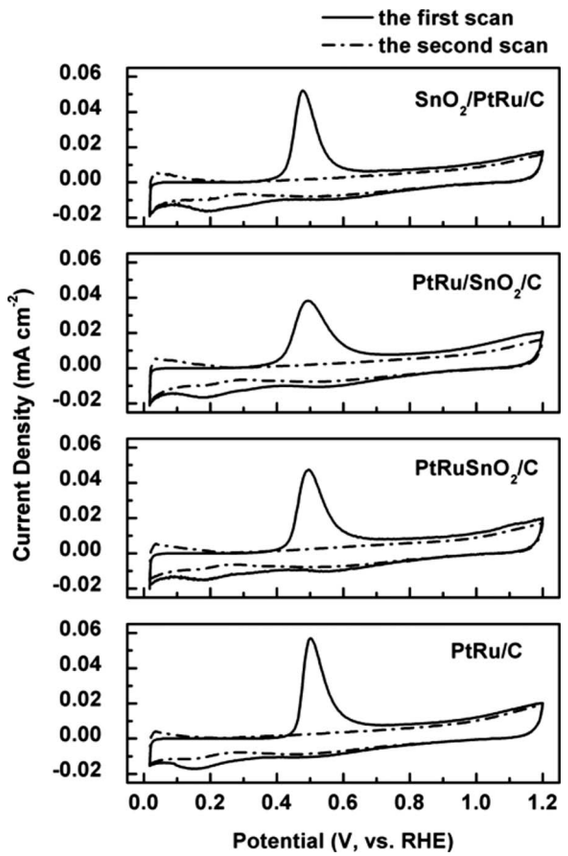

Figure 3. CO stripping voltammetries of PtRu/C and different SnO_2-modified PtRu/C catalysts in 0.5 M $HClO_4$ at 25°C. Scan rate: 10 mV s^{-1}.

PtRu/C and different SnO_2-modified PtRu/C catalysts, LSV curves with a slow scan rate of 1 mV s^{-1} were recorded and are presented in Fig. 5. The $PtRuSnO_2$/C catalyst showed a higher onset potential of methanol electro-oxidation than the PtRu/C catalyst, shifting positively by about 0.069 V, and the current density on the $PtRuSnO_2$/C catalyst was also poorer than that on the PtRu/C catalyst. Due to the lowest metal utilization in the $PtRuSnO_2$/C catalyst, a large fraction of Pt active sites was thought to be blocked by SnO_2,

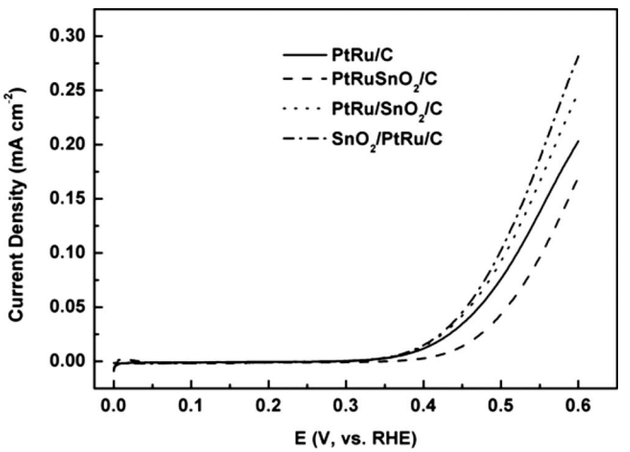

Figure 5. LSVs of methanol electro-oxidation of PtRu/C and different SnO_2-modified PtRu/C catalysts in 0.5 M $HClO_4$ + 0.5 M CH_3OH at 25°C. Scan rate: 1 mV s^{-1}.

which inhibited methanol adsorption and electro-oxidation.[10] The $PtRu/SnO_2$/C and SnO_2/PtRu/C catalysts exhibited a slightly lower onset potential and a superior activity compared with the PtRu/C catalyst. At an anode potential of 0.55 V, the current densities for methanol electro-oxidation on the $PtRu/SnO_2$/C and SnO_2/PtRu/C catalysts were 20 and 36% greater than those on the PtRu/C catalyst, respectively, while the current density on the $PtRuSnO_2$/C catalyst was 30% poorer than that on the PtRu/C catalyst.

The chronoamperometry measurement provided further information on the stability of the catalysts for methanol electro-oxidation. Figure 6 shows the current density–time curves at 0.55 V. Similar to the LSV results, the current densities of the chronoamperometry measurement decreased in the sequence of SnO_2/PtRu/C > $PtRu/SnO_2$/C > PtRu/C > $PtRuSnO_2$/C, in agreement with the CV and LSV results.

XPS characterization.— As described before, the $PtRuSnO_2$/C catalyst exhibits a negative effect of the addition of SnO_2, while the $PtRu/SnO_2$/C and SnO_2/PtRu/C catalysts show a positive effect of the addition of SnO_2, highlighting the importance of the SnO_2 deposition sequence in the SnO_2-modified PtRu/C catalyst preparation. XPS was performed to investigate whether the deposition sequence of SnO_2 affected the chemical state of Pt and Ru and the surface

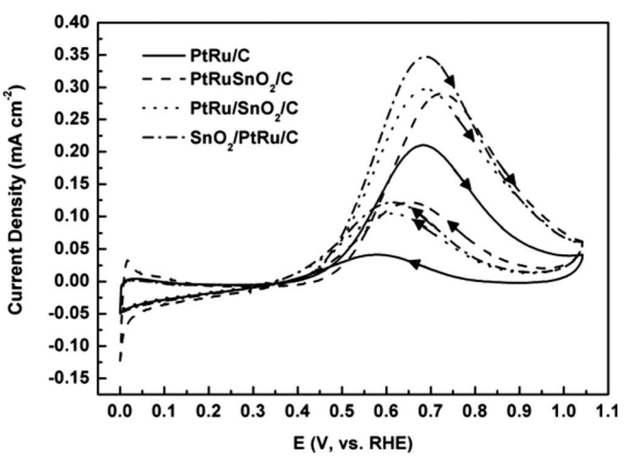

Figure 4. CVs of PtRu/C and different SnO_2-modified PtRu/C catalysts in 0.5 M $HClO_4$ + 0.5 M CH_3OH at 25°C. Scan rate: 20 mV s^{-1}.

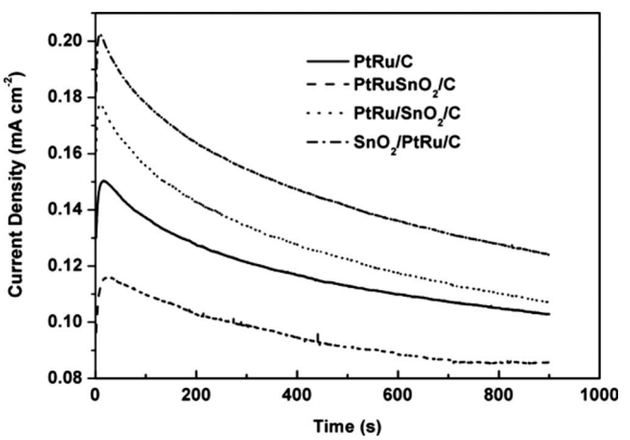

Figure 6. Chronoamperometry curves of PtRu/C and different SnO_2-modified PtRu/C catalysts at 0.55 V in 0.5 M $HClO_4$ + 0.5 M CH_3OH at 25°C.

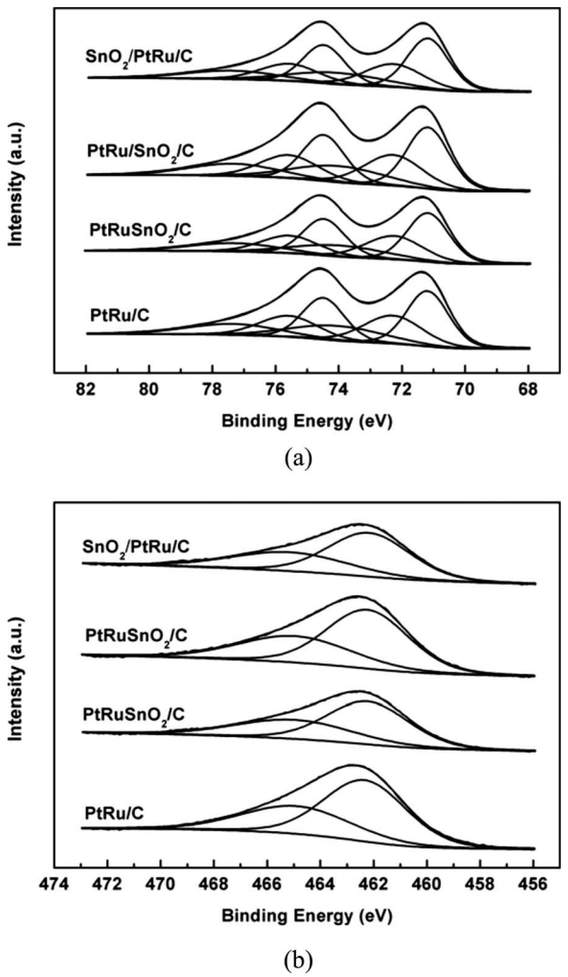

Figure 7. Pt 4f and Ru 3p signals in the XPS spectra of PtRu/C and different SnO_2-modified PtRu/C catalysts.

composition in the SnO_2-modified PtRu/C catalysts. Figure 7 shows the Pt 4f and Ru 3p spectra of the PtRu/C and different SnO_2-modified PtRu/C catalysts. The less intense Ru 3p region was analyzed instead of the main Ru 5d spectra, as the latter was overlaid with the C 1s region. The results obtained by deconvoluting the XPS spectra are summarized in Table II. The Pt $4f_{7/2}$ XPS line is fitted with a convolution of three peaks corresponding to three different Pt chemical states, as displayed in Fig. 7. The first peak (71.2 eV) is assigned to the reduced Pt (0) species, whereas the second peak (72.3 eV) is associated with oxidized Pt atoms from PtO species. The third peak (74.1 eV) is assigned to PtO_2 species.[28] The Ru $3p_{3/2}$ spectra could be deconvoluted into two components for Ru and RuO_2.[30] The XPS analysis result indicated that the deposition sequence of SnO_2 did not alter the chemical-state distribution of Pt and Ru but resulted in a different surface atomic ratio of Pt, Ru, and SnO_2 in the PtRu/C and SnO_2-modified PtRu/C catalysts, as listed in Table III. The ratio of Pt:Ru in the PtRu/C catalyst is 0.76:0.24, indicating that the polyol-synthesized PtRu/C catalyst was Pt rich in the catalyst surface because the surface tension of Pt is lower than that of Ru.[31,32] For all of the SnO_2-modified PtRu/C catalysts, the ratio of Pt:Ru was similar and greater than that of the PtRu/C catalyst regardless of the SnO_2 deposition sequence. The SnO_2 deposition sequence had a remarkable effect on the surface ratio of Sn despite the same nominal ratio, and the ratio of Sn decreased in the sequence of $SnO_2/PtRu/C > PtRuSnO_2/C > PtRu/SnO_2/C$. This agrees with the fact that the ratio of metals that were supported at the last step showed a relatively larger surface atomic ratio. The ratios of Sn in all the SnO_2-modified PtRu/C catalysts were larger than the nominal ratio, which coincided with previously reported results.[33,34] Although the SnO_2/PtRu/C catalyst has the largest surface ratio of Sn, the metal utilization, as listed in Table I, is still greater than that of the $PtRuSnO_2$/C and $PtRu/SnO_2$/C catalysts, also suggesting that the majority of SnO_2 particles in the SnO_2/PtRu/C catalyst were just in contact with PtRu particles.

In situ IRRAS measurement.— The $PtRuSnO_2$/C and SnO_2/PtRu/C catalysts exhibited the poorest and the greatest catalytic activity among the PtRu/C and SnO_2-modified PtRu/C catalysts; in situ IRRAS measurement was carried out to understand the molecular structures on the surface of PtRu/C, $PtRuSnO_2$/C, and

Table II. XPS analysis results obtained by curve fitting in Fig. 7.

Catalyst	Species	Binding energy (eV)	Peak half-width (eV)	Assignment	Atomic ratio (%)
PtRu/C	Pt $4f_{7/2}$	71.2	1.6	Pt	43.6
		72.3	2.2	PtO	30.9
		74.0	3.5	PtO_2	25.5
	Ru $3p_{3/2}$	462.3	3.6	Ru	62.7
		464.9	4.8	RuO_2	37.3
$PtRuSnO_2$/C	Pt $4f_{7/2}$	71.2	1.2	Pt	46.3
		72.2	2.4	PtO	30.5
		74.0	3.7	PtO_2	23.2
	Ru $3p_{3/2}$	461.2	3.2	Ru	61.2
		465.0	4.4	RuO_2	38.8
$PtRu/SnO_2$/C	Pt $4f_{7/2}$	71.2	1.6	Pt	44.2
		72.23	2.2	PtO	30.5
		74.0	3.4	PtO_2	25.3
	Ru $3p_{3/2}$	462.2	3.6	Ru	61.8
		464.9	5.0	RuO_2	38.2
SnO_2/PtRu/C	Pt $4f_{7/2}$	71.2	1.6	Pt	46.9
		72.3	2.2	PtO	29.5
		74.1	3.5	PtO_2	23.6
	Ru $3p_{3/2}$	462.2	3.6	Ru	61.9
		465.1	5.1	RuO_2	38.1

Table III. Surface atomic ratios of PtRu/C and different SnO_2-modified PtRu catalysts.

Catalyst	Surface atomic ratio		
	Pt	Ru	Sn
PtRu/C	0.76	0.24	0.0
$PtRuSnO_2/C$	0.50	0.14	0.36
$PtRu/SnO_2/C$	0.61	0.17	0.22
$SnO_2/PtRu/C$	0.45	0.12	0.43

SnO_2/PtRu/C catalysts during the electrocatalytic reaction. Figure 8 shows in situ IR spectra obtained in the 0.5 M $HClO_4$ + 0.5 M CH_3OH solution at (*i*) PtRu/C, (*ii*) PtRu/SnO_2/C, and (*iii*) SnO_2/PtRu/C, deposited on the gold substrate surface, in the potential region between 0.1 and 0.9 V. In the present work, the electrode potential was controlled at 0.05 V as soon as the electrolyte solution was introduced into the cell. As shown in Fig. 8a, almost no IR peak can be observed at 0.1 V, indicating that the oxidative decomposition rate of CH_3OH on the catalyst surface is very slow in the low potential region. A peak at 2040 cm^{-1} with a small shoulder at 1964 cm^{-1} is clearly observed at 0.2 V, and a broad band can also be identified at 1824 cm^{-1}. The peaks at 2040 and 1824 cm^{-1} are assigned to linearly adsorbed CO(CO_L) and bridge adsorbed CO(CO_B) on the Pt sites. The small shoulder at around 1964 cm^{-1} can be attributed to CO adsorbed on Ru sites (CO_{Ru}).[35-37] It is known that only one CO adsorption band is observed on the PtRu alloy surface, indicating that separated Pt and Ru phases should exist in the present PtRu/C catalyst,[38-41] which coincides with the low alloying degree of Ru in the PtRu/C catalyst, as listed in Table I. The CO_L intensity increases slightly with potential, while its peak position shifts to a higher frequency region, which can be attributed to the electron back-donation from the Pt to CO antibonding orbit. The band intensity and the position of the CO_{Ru} do not change much with potential. At 0.45 V, a peak appears at 2343 cm^{-1}, which can be assigned to the C–O stretching mode of CO_2, i.e., the final product for the CH_3OH electro-oxidation. The onset potential for the CO_2 formation is lower than that of the pure Pt electrode, suggesting that Ru works to oxidize CO from the OH_{ads} species through the bifunctional mechanism.[40] It is also interesting to note that the amount of the adsorbed CO is almost the same even when the CO_2 is produced continuously, implying that the catalyst surface is not deactivated by adsorbed CO species and that methanol is decomposed to CO_2 through intermediate CO with a certain rate in the potential region.[40]

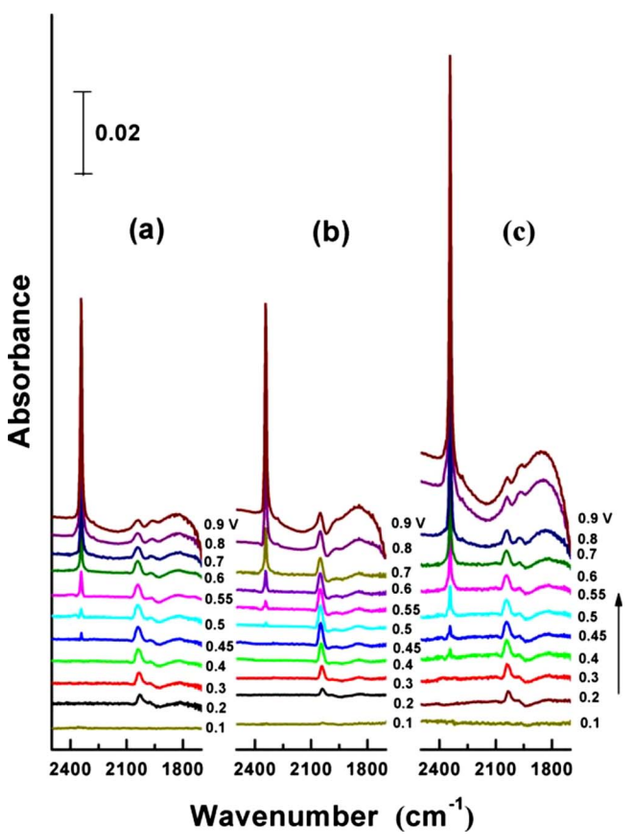

Figure 8. (Color online) In situ IRRAS spectra of (a) PtRu/C, (b) $PtRuSnO_2$/C, and (c) SnO_2/PtRu/C catalysts deposited on a gold substrate surface observed in 0.5 M $HClO_4$ + 0.5 M CH_3OH. Potentials are indicated on the right side of each spectrum; reference spectrum is recorded at 0.05 V.

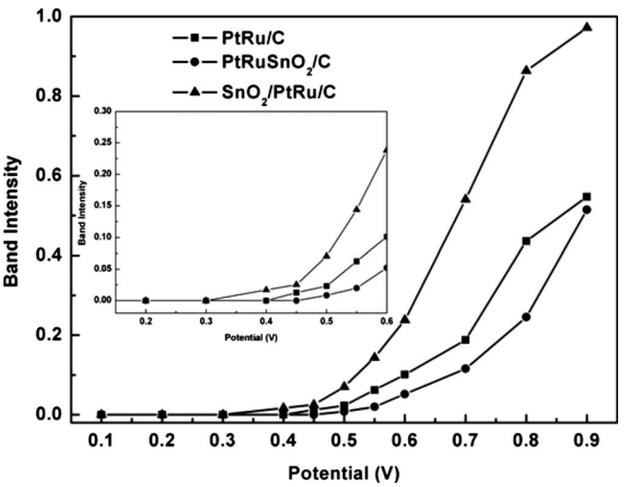

Figure 9. The integrated IR intensities for CO_2 generated as a function of electrode potential for PtRu/C, $PtRuSnO_2$/C, and SnO_2/PtRu/C catalysts.

In the case of the $PtRuSnO_2$/C catalyst (Fig. 8b), the spectral features are generally similar to that of the PtRu/C catalyst except the absence of CO_{Ru}, suggesting that these Ru sites may be blocked by SnO_2. This result agrees with the lowest PtRu metal utilization in the $PtRuSnO_2$/C catalyst as described above. In addition to CO adsorption bands on Pt sites, the SnO_2/PtRu/C catalyst (Fig. 8c) also shows CO_{Ru}. The IR peak positions for these CO species on the SnO_2/PtRu/C catalyst surface are quite similar to those of the PtRu/C catalyst. These results suggest that separated Pt and Ru phases are present on the catalyst surface, and this state is not affected by the later deposition of SnO_2 in the SnO_2/PtRu/C catalyst preparation. The onset potential for the CO_2 formation on the SnO_2/PtRu/C catalyst is ca. 0.4 V, lower than that on the PtRu/C and $PtRuSnO_2$/C catalysts. Figure 9 shows integrated IR intensities for CO_2 generated as a function of the electrode potential for the three catalysts. More CO_2 is formed on the SnO_2/PtRu/C catalyst surface, indicative of the greatest catalytic activity for methanol electro-oxidation among these catalysts. This result agrees with those shown in Figs. 4-6 in the same solution.

Proposed roles of SnO_2 in SnO_2-modified PtRu/C catalysts.— CO does not adsorb on the surface of SnO_2 particles, so the CO_{ads} formation does not interfere with the OH_{ads} formation on SnO_2 sites in contrast to the situation on Pt and Ru sites. In the CO stripping voltammetry, CO_{ads} poisoned the Pt and Ru sites, and OH_{ads} was formed on SnO_2 sites by a water-discharge reaction at a low potential, where OH_{ads} could not be formed on Pt and Ru sites. The

removal of CO_{ads} on Pt or Ru sites proceeded via its reaction with OH_{ads} on SnO_2 sites, so the onset potential of CO_{ads} electro-oxidation on all the SnO_2-modified PtRu/C catalysts was lower than that on the PtRu/C catalyst. Once CO_{ads} on Ru sites was electro-oxidized, OH_{ads} was produced on Ru sites at a faster rate than on SnO_2 sites. After the onset potential, CO_{ads} electro-oxidation on the SnO_2-modified PtRu/C catalyst could be maintained at a faster rate than that on the $PtSnO_2$/C catalyst with further increase in potential, so the peak potential of the CO_{ads} electro-oxidation on all the SnO_2-modified PtRu/C catalysts shifted negatively.

For methanol electro-oxidation, methanol was first adsorbed on Pt sites and then dehydrogenated step by step to produce CO_{ads}.[10] A large fraction of Pt sites covered by SnO_2 particles in the $PtRuSnO_2$/C catalyst were not facile for methanol adsorption and stepwise dehydrogenation, so both the onset and peak potentials of methanol electro-oxidation shifted positively compared with those on the PtRu/C catalyst, and the $PtRuSnO_2$/C catalyst showed a poorer catalytic activity for methanol electro-oxidation than the PtRu/C catalyst. During the methanol electro-oxidation, CO_{ads} also could migrate from Pt sites to Ru sites,[42] which competed with OH_{ads} formation on Ru sites, and the addition of SnO_2 into PtRu therefore provided an additional route for OH_{ads} formation, favoring methanol electro-oxidation. Because SnO_2 deposition did not affect the intimate contact of Pt and Ru particles on the carbon support and the alloyed Ru fraction, the SnO_2/PtRu/C catalyst showed the most pronounced promotional effect for methanol electro-oxidation among the three SnO_2-modified PtRu/C catalysts.

Conclusions

SnO_2-modified PtRu/C catalysts with different SnO_2 deposition sequences were prepared by the polyol process. XRD and STEM results indicated that the SnO_2 deposition sequence affected the particle size and alloyed Ru fraction of the SnO_2-modified PtRu/C catalysts. A simultaneous deposition of SnO_2 and PtRu or a prior deposition of SnO_2 onto the carbon support improved the metal dispersion and, at the same time, decreased the alloyed Ru fraction. The XPS result suggested that the deposition sequence of SnO_2 did not alter the chemical-state distribution of Pt and Ru but resulted in a different surface atomic ratio of Pt, Ru, and SnO_2. CO stripping voltammetry verified that the addition of SnO_2 into PtRu promoted CO_{ads} electro-oxidation in all the SnO_2-modified PtRu/C catalysts. Electrochemical measurements of methanol electro-oxidation exhibited that the catalytic activity decreased in the sequence of SnO_2/PtRu/C > PtRu/SnO_2/C > PtRu/C > $PtRuSnO_2$/C. In situ IRRAS results validated that the SnO_2/PtRu/C catalyst possessed the best catalytic activity for methanol electro-oxidation among these catalysts, exhibiting the lowest onset potential for CO_2 formation and the highest CO_2 band intensity. The same spectral features of CO adsorbed on the PtRu/C and SnO_2/PtRu/C catalysts suggested that the addition of SnO_2 did not affect the intimate contact of Pt and Ru particles in the SnO_2/PtRu/C catalyst preparation, which is crucial for obtaining a superior catalytic activity for methanol electro-oxidation.

Acknowledgment

This study was supported by the Strategic Development of PEFC Technologies for Practical Application Grant Program (grant no. 07003615-0) from the New Energy and Industrial Technology Development Organization (NEDO) of Japan. S.Y. acknowledges a Grant-in-Aid for Scientific Research (B) (no. 19350099) from MEXT.

Hokkaido University assisted in meeting the publication costs of this article.

References

1. M. P. Hogarth and T. R. Ralph, *Platinum Met. Rev.*, **46**, 146 (2002).
2. M. Watanabe and S. Motoo, *J. Electroanal. Chem. Interfacial Electrochem.*, **60**, 275 (1975).
3. T. Yajima, N. Wakabayashi, H. Uchida, and M. Watanabe, *Chem. Commun. (Cambridge)*, **2003**, 828.
4. C. Roth, A. J. Papworth, I. Hussain, R. J. Nichols, and D. J. Schiffrin, *J. Electroanal. Chem.*, **581**, 79 (2005).
5. P. Waszczuk, A. Wieckowski, P. Zelenay, S. Gottesfeld, C. Coutanceau, J.-M. Leger, and C. Lamy, *J. Electroanal. Chem.*, **511**, 55 (2001).
6. P. Waszczuk, G. U. Lu, A. Wieckowski, C. Lu, C. Rice, and M. I. Masel, *Electrochim. Acta*, **47**, 3637 (2002).
7. C. Roth, N. Benker, Th. Buhrmester, M. Mazurek, M. Loster, H. Fuess, D. C. Koningsberger, and D. E. Ramaker, *J. Am. Chem. Soc.*, **127**, 14607 (2005).
8. S. J. Liao, K. A. Holmes, H. Tsaprailis, and V. I. Birss, *J. Am. Chem. Soc.*, **128**, 3504 (2006).
9. K. I. B. Eguiluz, G. R. Salazar-Banda, D. Miwa, S. A. S. Machado, and L. A. Avaca, *J. Power Sources*, **179**, 42 (2008).
10. J. Zhu, F. Y. Cheng, Z. L. Tao, and J. Chen, *J. Phys. Chem. C*, **112**, 6337 (2008).
11. T. Kim, K. Kobayashi, M. Takahashi, and M. Nagai, *Chem. Lett.*, **34**, 798 (2005).
12. G. Siné, D. Smida, M. Limat, G. Fóti, and Ch. Comninellis, *J. Electrochem. Soc.*, **154**, B170 (2007).
13. M. K. Jeon, J. Y. Won, K. R. Lee, and S. I. Woo, *Electrochem. Commun.*, **9**, 2163 (2007).
14. C. Z. He, H. R. Kunz, and J. M. Fenton, *J. Electrochem. Soc.*, **144**, 970 (1997).
15. Z. Jusys, T. J. Schmidt, L. Dubau, K. Lasch, and L. Jörissen, *J. Power Sources*, **105**, 297 (2002).
16. M. V. Martínez-Huerta, J. L. Rodríguez, N. Tsiouvaras, M. A. Peña, J. L. G. Fierro, and E. Pastor, *Chem. Mater.*, **20**, 4249 (2008).
17. M. Arenz, V. Stamenkovic, B. B. Blizanac, K. J. Mayrhofer, N. M. Markovic, and P. N. Ross, *J. Catal.*, **232**, 402 (2005).
18. L. Jiang, L. Colmenares, Z. Jusys, G. Q. Sun, and R. J. Behm, *Electrochim. Acta*, **53**, 377 (2007).
19. Q. Wang, G. Q. Sun, L. H. Jiang, Q. Xin, S. G. Sun, Y. X. Jiang, S. P. Chen, Z. Jusys, and R. J. Behm, *Phys. Chem. Chem. Phys.*, **9**, 2686 (2007).
20. M. Götz and H. Wendt, *Electrochim. Acta*, **43**, 3637 (1998).
21. J. S. Guo, G. Q. Sun, S. G. Sun, S. Y. Yan, W. Q. Yang, J. Qi, Y. S. Yan, and Q. Xin, *J. Power Sources*, **168**, 299 (2007).
22. L. H. Jiang, G. Q. Sun, Z. H. Zhou, S. G. Sun, Q. Wang, S. Y. Yan, H. Q. Li, J. Tian, J. S. Guo, B. Zhou, et al., *J. Phys. Chem. B*, **109**, 8774 (2005).
23. D. C. Papageorgopoulos, M. Keijzer, and F. A. Bruijn, *Electrochim. Acta*, **48**, 197 (2002).
24. Y. Takasu, T. Fujiwara, Y. Murakami, K. Sasaki, M. Oguri, T. Asaki, and W. Sugimoto, *J. Electrochem. Soc.*, **147**, 4421 (2000).
25. S. Ye, A. Yashiro, Y. Sato, and K. Uosaki, *J. Chem. Soc., Faraday Trans.*, **92**, 3813 (1996).
26. S. Ye, T. Haba, Y. Sato, K. Shimazu, and K. Uosaki, *Phys. Chem. Chem. Phys.*, **1**, 3653 (1999).
27. S. Ye, Y. Sato, and K. Uosaki, *Langmuir*, **13**, 3157 (1997).
28. D. L. Wang, L. Zhuang, and J. T. Lu, *J. Phys. Chem. C*, **111**, 16416 (2007).
29. E. Antolini and F. Cardellini, *J. Alloys Compd.*, **315**, 118 (2001).
30. C. Bock, C. Paquet, M. Couillard, G. A. Botton, and B. R. MacDougall, *J. Am. Chem. Soc.*, **126**, 8028 (2004).
31. L. Colmenares, H. Wang, Z. Jusys, L. Jiang, S. Yan, G. Q. Sun, and R. J. Behm, *Electrochim. Acta*, **52**, 221 (2006).
32. V. Radmilović, H. A. Gasteiger, and P. N. Ross, Jr., *J. Catal.*, **154**, 98 (1995).
33. K. Ke and K. Waki, *J. Electrochem. Soc.*, **154**, A207 (2007).
34. E. M. Crabb, R. Marshall, and D. Thompsett, *J. Electrochem. Soc.*, **147**, 4440 (2000).
35. K. A. Friedrich, K. P. Geyzers, A. J. Dickinson, and U. Stimming, *J. Electroanal. Chem.*, **524–525**, 261 (2002).
36. S. Park, A. Wieckowski, and M. J. Weaver, *J. Am. Chem. Soc.*, **125**, 2282 (2003).
37. F. Maillard, G. Q. Lu, A. Wieckowski, and U. Stimming, *J. Phys. Chem. B*, **109**, 16230 (2005).
38. W. F. Lin, T. Iwasita, and W. Vielstich, *J. Phys. Chem. B*, **103**, 3250 (1999).
39. W. F. Lin, P. A. Christensen, A. Hamnett, M. S. Zei, and G. Ertl, *J. Phys. Chem. B*, **104**, 6642 (2000).
40. T. Iwasita, H. Hoster, A. John-Anacker, W. F. Lin, and W. Vielstich, *Langmuir*, **16**, 522 (2000).
41. F. Maillard, F. Gloaguen, F. Hahn, and J.-M. Léger, *Fuel Cells*, **2**, 143 (2002).
42. M. Metikoš-Huković and S. Omanović, *J. New Mater. Electrochem. Syst.*, **7**, 179 (2004).